Research Article

Frieder Reichenzer*, Stefan Dörr and Alois Herkommer

Transient simulation of laser beam propagation through turbulent cutting gas flow

https://doi.org/10.1515/aot-2018-0070
Received December 16, 2018; accepted February 22, 2019; previously published online April 2, 2019

Abstract: For many laser machining applications, an assist gas is required. However, for applications with high pressure or temperature gradients, the density of the assist gas is not homogeneous. Thus, the laser propagation is influenced by the density properties within the turbulent gas. In this article, an overview and example results of the influence of a nozzle geometry on the light propagation in two dimensions are presented.

Keywords: CFD; laser; multiphysics.

1 Introduction

In this study, we present a combination of fluid mechanics and computational beam propagation as a method to determine the effect of a fluid on a laser cutting process. The focus of this article lies on the fast alterations of the properties of a laser beam depending on the turbulent flow field of the fluid through a nozzle. The propagation of the laser light is dependent on the optical properties of the medium it passes through. While it is possible to calculate the light propagation rigorously via the Maxwell equations, it is often times not expedient because of the high computational cost. In order to reduce this computational effort, different schemes for calculating the influence of the fluid on the beam propagation are possible, and the generated information on these schemes varies extremely. A more statistical approach is heavily used for aero-optics, which has a strong focus on the effects of flows around turrets on the beam propagation between two airplanes [1, 2]. For the optical evaluation of their fluid studies, the most often used approach is the calculation of the optical path difference for the system [3–5]. The far-field distortions are calculated via ray tracing or fourier optics, starting from the optical path difference disturbances [6–8]. Another field where the light-fluid interaction is investigated numerically is laser welding. For those applications, the multiphysics approach is used to model the light-matter interaction and the energy deposited into the matter from the absorbed laser light. The tools used range from the modeling of the light via the radiative transfer equation [9, 10] to coupling a ray tracing algorithm to an advanced particle method [11].

Because of the recent activities in the use of simulations in the optimization of laser cutting and the experimental investigation of beam shaping and movement during the laser cutting process [12–15], we would like to show in this article that the influence of the assist gas should not necessarily be neglected.

In order to estimate the effects of the cutting gas on the laser light propagation, the presented study builds upon the results of a prior investigation into the flow field inside a two-dimensional (2D) representation of a laser cutting nozzle [16]. Using the same geometry as in the current study (Figure 1), it was shown via computational fluid dynamic calculations and Schlieren experiments that jet-driven oscillations occur at pressures used for laser fusion cutting. It was shown that the behavior of the flow field and the oscillation frequency is dependent on the position and angles of the inlets relative to each other and the geometry boundaries.

Because the oscillations occur without any feedback loop inside a closed geometry, the results can be linked to other studies where similar effects were studied experimentally [17–21] and computationally [22–29] in a geometry conceived by Raghu [30].

Here, we present an overview and example results of the light propagation through the flow field inside a laser nozzle which displays transient and turbulent behavior. For the presented simulations, only the OpenSource software

***Corresponding author: Frieder Reichenzer,** Institute of Applied Optics, University of Stuttgart, Pfaffenwaldring 9, 70569 Stuttgart, Germany; and TRUMPF Laser- und Systemtechnik, Johann-Maus-Str. 2, 71254 Ditzingen, Germany, e-mail: f.reichenzer@live.com
Stefan Dörr: TRUMPF Laser- und Systemtechnik, Johann-Maus-Str. 2, 71254 Ditzingen, Germany
Alois Herkommer: Institute of Applied Optics, University of Stuttgart, Pfaffenwaldring 9, 70569 Stuttgart, Germany

www.degruyter.com/aot
© 2019 THOSS Media and De Gruyter

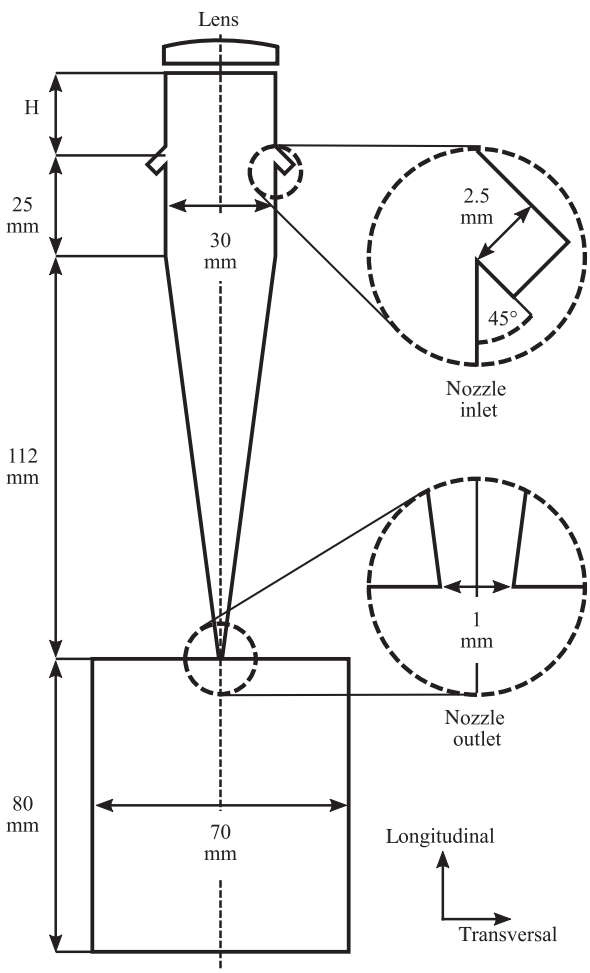

Figure 1: Nozzle design used in this study, with inlets to the geometry symmetrical to the center line.

was used. For the fluidic simulations, the OpenSource library OpenFoam was used, and the used beam propagation method (BPM) was implemented in Python.

2 Geometry

The geometry used in this study was derived from a typical nozzle used for high-pressure laser machining applications, as illustrated in Figure 1. The geometry consists of a rectangular area with two inlets, a converging nozzle and an outflow region connecting to ambient conditions. The light is focused and propagates from the top, where a lens is sketched, through the geometry and through the nozzle throat to the outlets. Assuming the light source and beam propagation up to the lens are constant, the beam properties at the focal point are dependent on the focal length of the lens. For laser fusion cutting applications, the focal point is generally positioned a few mm below the nozzle throat. Therefore, the overall length of the geometry is determined by the focal length of the lens used. In this study, the length of the geometry is varied via the distance between the inlets and the lens H.

3 Simulations

3.1 Fluid simulation

The optical properties of the medium are calculated based on fluid simulations using the open source software library OpenFoam, version 3.0.x, as described in [16]. Out of this library, the rhoCentralFoam, a two-step time-splitting algorithm with a second-order upwind scheme discretization, was used. With this solver, the compressible and transient behavior was calculated with time steps at the order of $\Delta t \approx 10^{-9}$ s. To account for turbulence, the k-ω-SST model was employed. Because of its use in the application, nitrogen, as a compressible and ideal gas, is used as the fluid. As the initial condition, a fixed total pressure is applied to the inlets. The outlets at the sides and bottom of the outflow region are modeled with a zero-gradient/fixed value boundary condition for the outflow/inflow (Figure 1). A no-slip boundary condition is applied to the walls using the respective wall functions to calculate the turbulence parameters. The calculations are conducted on an unstructured hex mesh created via the application *cartesian2DMesh* by creativeFields.

3.2 Optical simulation

For the optical simulations, a BPM algorithm is implemented in Python. The computations follow in general the directions described by Schmidt [31]. For the BPM propagation, the refractive index field is partitioned into several equally sized slices in the direction of the propagation. For each step, a phase term calculated from the refractive index field is multiplied to the incoming lightfield. This light field is then propagated via Fourier propagation to the next slice. Starting from a ground mode Gaussian beam distribution, the effects of flow field on the laser propagation can be calculated. The refractive index for the phase term is determined via the Gladstone-Dale formula:

$$n(x, y, z) = 1 + (1 - n_0)\frac{\rho(x, y, z)}{\rho_0} \tag{1}$$

with a reference refractive index n_0 for a reference density ρ_0 (Figure 2). As the point of reference, standard conditions (temperature 273 K, pressure 1013 hPa) were chosen with a value of $n_0 - 1 = 2.9 \times 10^{-4}$ [32].

The BPM implementation used in this study requires an equidistant mesh with 2^N elements in the transversal direction. Because of this, the unstructured data from the fluid simulation are mapped onto a structured mesh with linear interpolation. The resolution of this mesh is 1 µm in the transversal direction and 19 µm in the longitudinal direction. For the input field, a collimated Gaussian beam with a beam radius $\omega_0 = 5$ mm is used at a wavelength of 1.0 µm. To this complex light field, a phase is applied which leads to a focal point at 1 mm below the nozzle in the longitudinal direction. The position $\bar{x}$ in the transversal direction and radius ω are calculated via the first and second moments, respectively:

$$\bar{x}(z) = \frac{1}{\int_{-\infty}^{\infty} I(x)dx} \int_{-\infty}^{\infty} x \cdot I(x)dx \tag{2}$$

$$\omega^2 = 4\sigma^2 = \frac{4}{\int_{-\infty}^{\infty} I(x)dx} \int_{-\infty}^{\infty} (x - \bar{x})^2 \cdot I(x)dx \tag{3}$$

The position of the beam waist is then calculated from the minimum of ω in the longitudinal direction. Because this study is motivated by the potential effects on the laser workpiece interaction, the beam radius and transversal position are presented at the position of the beam waist at standard conditions set at 1 mm below the nozzle. For different distances between the inlets and the lens H, this leads to a difference in the divergence angle and beam waist radius ω_0.

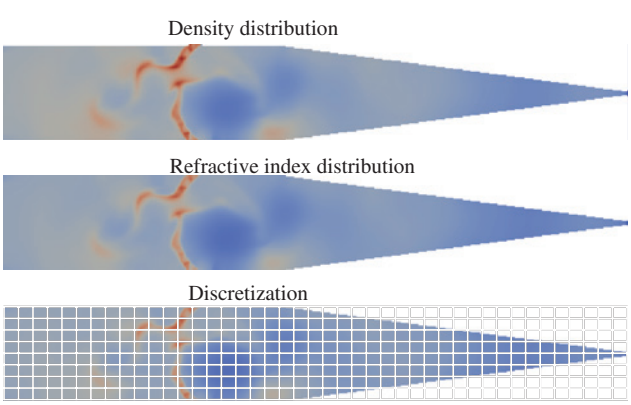

Figure 2: Density distribution, refractive index distribution and discretization of refractive index distribution.

4 Results

4.1 Behavior of fluid

In the presented geometry, as shown by [16], the behavior of the flow field is dominated by the creation of vortices driven by the jet flow. Dependent on the distance between the inlet and the lens H, the flow field is in a stationary state, displays symmetrical or asymmetrical oscillation as shown in Figure 3 and is characterized by the oscillation period T. Starting from a stationary state, an increase in the value of H leads to symmetrical oscillations (Figure 3A–C), and a decrease in the period time

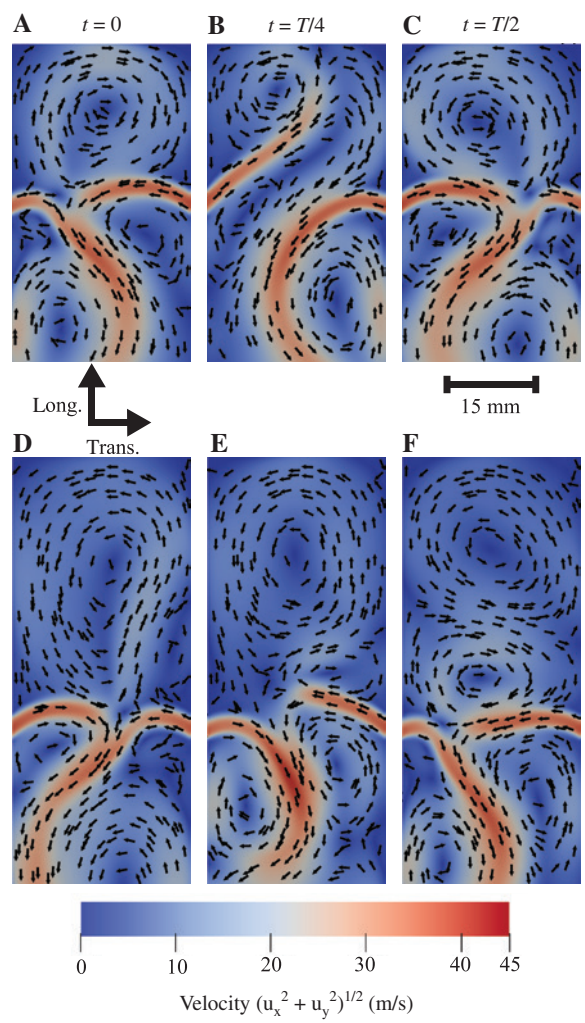

Figure 3: Oscillations of the simulated flow field for different values of H. (A–C) Flow field for $H = 26.25$ mm from numerical calculation for one half oscillation period $T/2$. (D–F) Flow field for $H = 45$ mm from numerical calculation for one half oscillation period $T/2$. Arrows indicate direction of flow along lines.

T, an order of magnitude 10 ms. The symmetry refers to the possibility of transferring between flow fields with a temporal difference $\Delta t = T/2$ by mirroring them in the transversal direction. At a certain value of H, the flow fields at $t = 0$ and $t = T/2$ (Figure 3D–F) display no mirror symmetry above the inlets, making the oscillation asymmetrical. The change from symmetrical to asymmetrical oscillations by increasing the value of H is assumed to be linked to a mechanism found in lid-driven cavities [33]. After reaching the asymmetric oscillation state, T is independent of H. In this study, this behavior was captured by both the Schlieren experiments and the fluidic simulations as presented in this article. While the simulations captured the qualitative behavior correctly, they result in a 2.4(4) larger period time. This is due to the 2D character of the simulation as compared to the real 3D geometry [24, 29].

4.2 Influence on light propagation

In order to study the effects of the flow field on the optical propagation, we in the following concentrate on two situations: $H = 18.75$ mm, safely in the symmetrical flow regime, and $H = 45$ mm, deep in the asymmetric regime.

Same as for the flow field, the different oscillatory states are present in the refractive index distribution, calculated via Eq. (1). At the positions of the vortices, the refractive index is smaller relative to its surroundings due to the decreased pressure and, therefore, the density. At points where the flow of the gas jets intersect, the points of impingement, the fluid is compressed locally, which leads to a higher density and therefore an increased refractive index in this area. For $H = 18.75$ mm, the position of the point of impingement changes the high-n area from left at $t = 0$ to right at $t = T/2$ symmetrically in the transversal direction. At the most extreme positions, the point of impingement is pushed outside of the beam propagation path. Under the inlet jets toward the downstream, the vortex/low-n area gets bigger and is pushed into the light path. After that, it stays in the light path and is pulled downstream toward the nozzle. This leads to an oscillation of the beam displacement in the transversal direction at the position of the workpiece with an amplitude of 3 µm and a period time of $T = 13$ ms (Figure 6, dotted line). The maximum beam displacement relative to the beam radius is at around 27% with a mean beam displacement of −0.1 µm over one period T. This is accompanied by an oscillating beam radius at the position of the workpiece with an amplitude of 0.4 µm. While the change in the oscillatory state leads to a sign change in the beam displacement, its effects on the beam radius are the same, leading to oscillations at half the period time T.

In Figures 4 and 5, the asymmetry of the flow field is apparent in the density field for $H = 45$ mm as well. In this case, the impingement point only moves out of the light path when the area above the inlets includes two counter-rotating similar-sized vortices. At $t = T/2$, where the area above the inlet is filled with only one vortex, the impingement point is still inside the beam

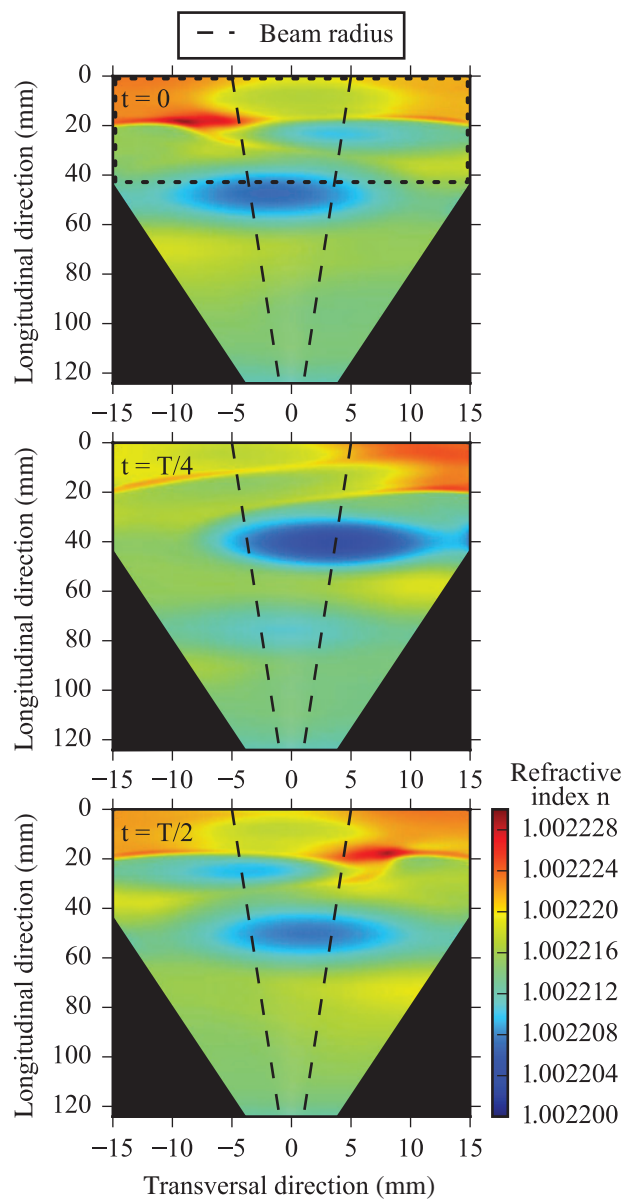

Figure 4: Simulation of the refractive index for $H = 18.75$ mm. Dashed lines indicate beam radius.

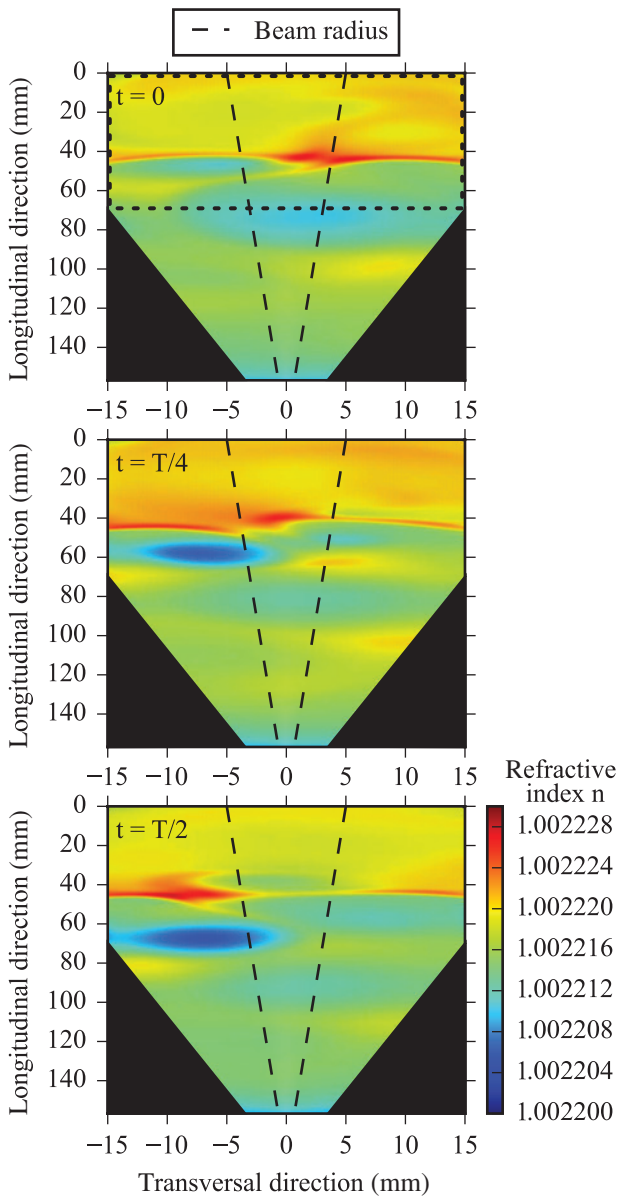

Figure 5: Simulation of the refractive index for $H = 45$ mm. Dashed lines indicate beam radius.

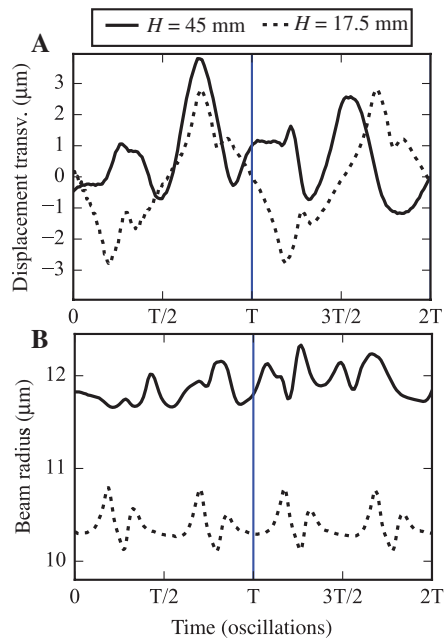

Figure 6: Time-dependent behavior of beam properties (at the workpiece position). (A) Beam position in transversal direction at the workpiece position. (B) Beam radius at the workpiece position. Solid line: $H = 45$ mm, dotted line: $H = 18.75$ mm.

radius. As a result of this, the transverse position does not oscillate around a position of zero beam displacement but around a mean value of 0.6 µm (see Figure 6A). Because the size ratio of the two vortices above the inlet changes between two full oscillations, the amplitude varies over time with the maximum beam displacement relative to the beam radius at 31%. While for the transversal beam position a periodicity can still be found, this breaks down for the beam radius at $H = 45$ mm (Figure 6B). Because of the change in size of the vortices above and below the inlets, the change of the beam radius is random.

5 Discussion

By applying an optical simulation to the results of a fluid simulation, the effects of the geometry on the beam properties can be made accessible. The results of this study in 2D indicate that the deviation of the beam position from its initial position is significant at 30% relative to the beam radius and non-negligible at small time scales, in this case 10–18 ms. For processes with integration times far grater than the oscillation period and a flow field displaying symmetrical oscillations, the beam movement could be modeled statically with a slightly larger mean beam radius rather than the instantaneous beam radius. For a nozzle geometry displaying non-symmetric oscillations, this is not possible. Because of the non-deterministic nature of the asymmetry, the mean position on the workpiece can change between two measurements. Therefore, a process, which relies on the position of the beam, would have to take the displacement into account. Additionally, the asymmetry can break and change and switch sides during a process. This leads to a modulation of the beam position at time scales greater than the period time of the oscillations. As laser processes are more and more optimized for speed and stability, effects due to the process gas will have to be taken into account. This is especially true for laser sources with high brilliance. Because smaller spot

sizes on the workpiece are possible, changes in the beam position become more pronounced. In general, the combination of fluid simulations and optical simulations can, thus, lead to process improvements for high-pressure and high-precision applications.

References

[1] S. Gordeyev and E. Jumper, Prog Aerosp. Sci. 46, 388–400 (2010).
[2] E. J. Jumper and S. Gordeyev, Annu. Rev. Fluid Mech. 49, 419–441 (2017).
[3] H. Ayyalasomayajula, S. Arunajatesan, C. Kannepalli and N. Sinha. Large eddy simulation of a supersonic flow over a backward-facing step for aero-optical analysis. In Aerospace Sciences Meetings. American Institute of Aeronautics and Astronautics, January 2006.
[4] H. J. Catrakis and R. C. Aguirre, AIAA J. 42, 1973–1981 (2004).
[5] K. Wang and M. Wang. J. Fluid Mech. 696, 122–151 (2012).
[6] A. Mani, M. Wang and P. Moin. Computational study of aero-optical distortion by turbulent wake. In Fluid Dynamics and Co-located Conferences (American Institute of Aeronautics and Astronautics, Toronto, Ontario, Canada, June 2005).
[7] M. Wang, A. Mani and S. Gordeyev, Annu. Rev. Fluid Mech. 44, 299–321 (2012).
[8] H. Xiao and Z. Fan. Appl. Opt. 49, 5049–5058 (2010).
[9] S. Chandrasekhar, in 'Radiative Transfer', Ed. By D. Morton (Dover publications, New York, 1960).
[10] A. Otto, H. Koch, K.-H. Leitz and M. Schmidt, Physics Procedia, 12:11–20, 2011. Lasers in Manufacturing 2011 – Proceedings of the Sixth International WLT Conference on Lasers in Manufacturing.
[11] H. Hu, F. Fetzer, P. Berger and P. Eberhard, GAMM-Mitteilungen 39, 149–169 (2016).
[12] S. S. Kudesia, W. S. O. Rodden, D. P. Hand and J. D. C. Jones, ICALElO 2001, 1439–1448 (2001).
[13] G. C. Rodrigues and J. R. Duflou. J. Phys. D Appl. Phys. 51, 065601 (2018).
[14] H. Tercan, T. Al Khawli, U. Eppelt, C. Büscher, T. Meisen, et al., Procedia CIRP 52, 292–297 (2016).
[15] G. Yang, L. Liu, Z. Jiang, J. Guo and T. Wang, Optik 156, 148–154 (2018).
[16] F. Reichenzer, M. Schneider and S. Dörr, AIAA J. 56, 4768–4774 (2018).
[17] V. A. Denshchikov, V. N. Kondrat'ev and A. N. Romashov, Fluid Dyn. 13, 924–926 (1978).
[18] V. A. Denshchikov, V. N. Kondrat'ev, A. N. Romashov and V. M. Chubarov, Fluid Dyn. 18, 460–462 (1983).
[19] J. W. Gregory, J. P. Sullivan and S. Raghu, J. Vis. 8, 169–176 (2005).
[20] J. W. Gregory, J. Sullivan, G. Raman and S. Raghu, Characterization of a micro fluidic oscillator for flow control. In 2nd AIAA Flow Control Conference (American Institute of Aeronautics and Astronautics, Portland, OR, 2004) p. 2692.
[21] J. W. Gregory, J. P. Sullivan, G. Raman and S. Raghu, AIAA J. 45, 568–576 (2007).
[22] J. W. Gregory and M. N. Tomac. A review of fluidic oscillator development and application for flow control. In 43rd Fluid Dynamics Conference (American Institute of Aeronautics and Astronautics, San Diego, CA, USA, 2013).
[23] S. D. Heister, S. Bidadi and Y. Matsutomi. Atomization Sprays 21, 127–138 (2011).
[24] E. J. Meier and S. D. Heister, Int. J. Flow Control 7, 19–36 (2015).
[25] R. P. Pawlowski, A. G. Salinger, J. N. Shadid and T. J. Mountziaris, J. Fluid Mech. 551, 117–139 (2006).
[26] S. Raghu, Exp. Fluids 54, 1455 (2013).
[27] M. N. Tomac and J. Gregory. Frequency studies and scaling effects of jet interaction in a feedback-free fluidic oscillator. In 50th AIAA Aerospace Sciences Meeting including the New Horizons Forum and Aerospace Exposition, Aerospace Sciences Meetings (American Institute of Aeronautics and Astronautics, June 2012).
[28] M. N. Tomac and J. W. Gregory, Exp. Fluids 55, 1730 (2014).
[29] M. N. Tomac. Internal fluid dynamics and frequency characteristics of feedback-free fluidic oscillators. PhD thesis, The Ohio State University, 2013.
[30] S. Raghu. Feedback-free fluidic oscillator and method, July 3 2001. US Patent 6, 253, 782.
[31] J. D. Schmidt. Numerical simulation of optical wave propagation with examples in MATLAB, volume PM199. SPIE, Bellingham, Washington, USA, July 2010.
[32] E. R. Peck and B. N. Khanna, J. Opt. Soc. Am. 56, 1059–1063 (1966).
[33] F. Pan and A. Acrivos, J. Fluid Mech. 28, 643–655 (1967).